2003

Modeling Moving Droplets: A Precursor Film Approach

Benjamin Bryant
Harvey Mudd College

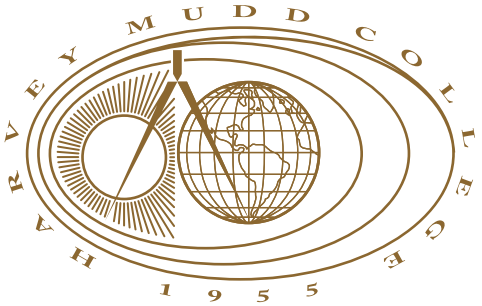

Modeling moving droplets:
A precursor film approach

by
Benjamin P. Bryant
Andrew Bernoff and Anette Hosoi, Advisors

Advisor: _____

Advisor: _____

May 2003

Department of Mathematics

HARVEY MUDD
COLLEGE

Abstract

Modeling moving droplets:

A precursor film approach

by Benjamin P. Bryant

May 2003

We investigate the behavior of moving droplets and rivulets, driven by a combination of gravity and surface shear (wind). The problem is motivated by a desire to model the behavior of raindrops on aircraft wings. We begin with the Stokes equations and use the approximations of lubrication theory to derive the specific thin film equation relevant to our situation. This fourth-order partial differential equation describing the height of the fluid is then solved numerically from varying initial conditions, using a fully implicit discretization for time stepping, and a precursor film to avoid singularities at the drop contact line. Results describing general features of droplet deformation, limited parameter studies, and the applicability of our implementation to the long-term goal of modeling wings in rain are discussed.

Table of Contents

List of Figures

Acknowledgments

Thanks are due to Professors Bernoff and Hosoi for their guidance, to Joe Malone and Dmitriy Kogan for their helping me get over the initial hurdles of learning C, and of course, to my parents.

Chapter 1

Introduction

The behavior of thin films, droplets and rivulets is of interest in many applications. These include such diverse areas as coating flows used in the creation of microchips and other electronic devices, sintering in metallurgy, spray coating processes, heat exchange, and oil recovery [15, 4]. We are motivated by the problem of water flowing on an aircraft wing or other possibly inclined surfaces sheared by wind. In this problem, droplets accumulate on the surface as a result of rain impacting the wing. They are then sheared by the wind and coalesce into a spanwise film, which is convected back along the wing, and eventually breaks up into rivulets, which are driven farther back off the wing or break up into larger drops, which in turn run off the wing's trailing edge. The presence of this phenomenon on the wing surface has generally undesirable effects on wing performance, in that it tends to decrease lift and increase drag under most flight conditions [2, 13, 12].

Thompson found in wind tunnel tests that performance degradation correlates with increasing contact angle (and therefore decreasing surface wettability), presumably due to the flatter profile presented by wetting films [14]. He also found that wetting surfaces gave rise to longer convecting regions, but that for a given contact angle, a longer film convection region more negatively affected performance than a short region. This implies that an optimal method for alleviating degradation in flight performance is to use a wettable surface, but take steps to minimize the length of the film convection region, perhaps by controlling the ac-

tion of the droplets prior to their coalescing into a film.

This leads to the need for modeling the motion of a droplet subjected to surface shear from the surrounding gas while experiencing a body force due to gravity, which is the primary aim of this thesis. In the remainder of chapter 1, we will discuss previous efforts related to this problem and briefly describe our approach. In chapter 2 we derive the relevant equations to describe the situation we are modeling. Chapter 3 outlines the numerical methods used to implement our model. In chapter 4 we discuss results, before concluding in chapter 5 with a summary and suggestions for future work.

1.1 Previous work

Drops and rivulets have previously been modeled in many different situations, using many different techniques. Most relevant to our aim is the work of Durbin [5], who developed a model describing the shape of a drop being sheared by a high-Reynolds number stream. However, he solves this using only a pressure distribution, ignoring shear by assuming the droplet is of equal or greater thickness than the boundary layer. In the less aeronautical regime, Wilson et al [15] analytically examined a non-Newtonian fluid driven by gravity or shear stress using a contact line model and certain lubrication approximations. They obtained similarity solutions for two-dimensional steady profiles in the transverse direction, in the limits of strong and weak surface tension.

Moriarty and Schwartz [9] developed a precursor film model of a droplet running down an inclined surface that they modified to account for shear effects as well. Their model uses the method of matched asymptotic expansions, accounting for surface tension only at the critical area near the front of the advancing drop, where curvatures are highest. They then match this with a simpler model for the flatter, receding face of the drop. A larger issue with their model is that

their equations describe height as a function of time and one spatial dimension only, and therefore are in reality modeling ridges of fluids and not drops. (For future reference, this sort of modeling is referred to as one-dimensional. It should be noted that, because the independent variables in the model are used to track a height, one-dimensional modeling produces two-dimensional drops, and two-dimensional modeling results in three-dimensional drops.)

Li and Pozrikidis [8] modeled a droplet adhering to a surface surrounded by Stokes flow. While an interesting problem, this is quite distinct from our aims, because they modeled two immiscible fluids of equivalent viscosity, as opposed to a liquid-gas interface. Also, their model uses a pinned contact line, and therefore it is impossible for the drop to move. Schleizer and Bonnecaze [11] used a boundary-integral method to study a drop between two plates subject to pressure or shear stress. Their model is also one-dimensional, and explicitly tracks a moving contact line. It is not, therefore, what we are seeking to do, but will prove useful in making comparisons after our model is developed. Lastly, Dimitrakopoulos and Higdon [4] studied the conditions required for the displacement of a two-dimensional droplet from a surface, using a contact line model.

Our aim is to track the height of a shearing droplet as a function of time and two spatial dimensions, and it appears this has so far not been done.

1.2 Our methods

Our approach to the problem is to restrict our attention to very wetting drops, and utilize the simplifications of lubrication theory. Thus we assume our drops are governed by the well-studied thin film equation. For our situation it takes the form

$$h_t = \nabla \cdot \left[\frac{h^3}{3} \nabla \left(Gh - S\nabla^2 h \right) \right] + \left(\Gamma h^3 + Ch^2 \right)_x , \tag{1.1}$$

where h is the height of the fluid and each term represents a contribution from different forces, which are detailed in the derivation found in chapter 2. The above

equation is a specific example of the more general class of thin film equations, which have been modeled fairly extensively in the context of lubrication theory, where it is usually presented in it's one dimensional form [10, 6]. We plan to, among other things, test it's applicability to droplet modeling.

The primary goal of our research is to successfully simulate droplet deformation under both gravity and surface shear stresses, describing height as a function of time and two spatial dimensions. This will be accomplished by numerically solving the applicable thin film PDE, using a precursor film to account for contact line singularities. We will also examine the potential of this method of implementation for larger-scale modeling of droplets on a wing. Numerical details, results and further goals are discussed in later chapters. First however, we must derive the equation we plan to model.

Chapter 2

Derivation of Relevant Equations

2.1 Fundamental equations

We begin with the Stokes equations which describe flow at very low Reynolds numbers, and derive the thin film equation relevant to our situation. The Stokes equations are the Navier-Stokes equations with the inertial and time-derivative terms removed, since they are assumed to make a neglible contribution relative to the terms we consider, which are those describing pressure gradients, shear motion, and body forces:

$$\nabla p = \mu \nabla^2 \mathbf{u} + \mathbf{F}, \tag{2.1}$$

where the body force $\mathbf{F}$ is simply the force due to gravity.

For our purposes, we assume gravity can act in the z and x direction only. This allows us to model flow on a plane inclined at any angle, with z normal to the surface of the plane. Taking this into account and expanding the above equation into separate parts, we have

$$p_x = \mu(u_{xx} + u_{yy} + u_{zz}) + \rho g \sin\theta \tag{2.2}$$

$$p_y = \mu(v_{xx} + v_{yy} + v_{zz}) \tag{2.3}$$

$$p_z = \mu(w_{xx} + w_{yy} + w_{zz}) - \rho g \cos\theta, \tag{2.4}$$

where u,v and w are the x,y and z components of $\mathbf{u}$ respectively, θ is the angle of inclination below horizontal (that is, positive θ indicates sloping down to the right), and subscripts denote partial differentiation with respect to the subscripted

variable. Also, for convenience, the x and z gravity terms $\rho g \sin\theta$ and $\rho g \cos\theta$ will from hereon be referred to as just M and N, respectively.

In wetting film and droplet applications such as ours, we recognize that the characteristic height (H) is different (specifically, much much less) than than the length (L) for variation in x and y. To further simplify the equations, we take advantage of this relation by examining the relative scales of elements of the $\nabla^2\mathbf{u}$ term. We partially nondimensionalize by assigning

$$x = Lx, y = Ly, z = \epsilon Lz, t = Tt \tag{2.5}$$

where $\epsilon = \frac{H}{L} \ll 1$ (this is known as the thin film approximation) and variables appearing on the right side of the equation are nondimensional.

Substituting these gives:

$$\begin{aligned} p_x &= \frac{\mu}{LT}(u_{xx} + u_{yy} + \frac{1}{\epsilon^2}u_{zz}) - M & (2.6)\\ p_y &= \frac{\mu}{LT}(v_{xx} + v_{yy} + \frac{1}{\epsilon^2}v_{zz}) & (2.7)\\ p_z &= \frac{\mu}{LT}(\epsilon w_{xx} + \epsilon w_{yy} + \frac{1}{\epsilon}w_{zz}) - N, & (2.8) \end{aligned}$$

From this, we see that among the terms contained in $\nabla^2\mathbf{u}$, u_{zz} and v_{zz} are dominant, since all others are at least $O(\epsilon)$ smaller, and most are smaller still. Retaining these terms of the original equations leaves us with governing equations of:

$$\begin{aligned} p_x &= \mu u_{zz} + M & (2.9)\\ p_y &= \mu v_{zz} & (2.10)\\ p_z &= -N, & (2.11) \end{aligned}$$

and also the continuity equation,

$$u_x + v_y + w_z = 0. \tag{2.12}$$

The boundary conditions are determined by the specific situation we are trying to model, which will be discussed below.

2.2 Thin film equation derivation

We model the effect of wind flowing past by simply imposing a constant shear stress in the x direction at the free surface, and a zero shear stress in the y direction at the surface. This is expressed as $\mu u_z = C$ and $\mu v_z = 0$, at h, the height of the film. We also must account for pressure differences due to surface curvature. Since we are utilizing the lubrication approximation, it is valid to assume that the curvature is small, and thus use $\nabla^2 h$ as the first order approximation to curvature. Thus at the surface we also have $p = -\sigma\nabla^2 h$, where σ is the surface tension coefficient, and the Laplacian is two-dimensional. At the fluid-solid interface, we have the standard no-slip condition, $\mathbf{u} = 0$. Expressed together, we have:

$$z = h \quad : \quad \mu u_z = C, \qquad \mu v_z = 0, \qquad p = -\sigma\nabla^2 h \tag{2.13}$$

$$z = 0 \quad : \quad \mathbf{u} = 0, \tag{2.14}$$

Integrating (2.11) with respect to z and satisfying the surface tension boundary condition, we find

$$p = -N(z - h) - \sigma\nabla^2 h. \tag{2.15}$$

We then differentiate with respect to x and equate it with (2.10) giving

$$\mu u_{zz} = (Nh - \sigma\nabla^2 h)_x - M. \tag{2.16}$$

Integration with respect to z and satisfaction of boundary conditions gives:

$$\mu u_z = [-(M + (-Nh + \sigma(\nabla^2 h))_x)](z - h) + C \tag{2.17}$$

Here C is the shear coeffecient, not a constant of integration.

Integrating one more time, we arrive at an expression for u:

$$u = \frac{1}{\mu}\left[\left[-(M + (-Nh + \sigma(\nabla^2 h))_x)\right](\frac{1}{2}z^2 - hz) + Cz\right]. \tag{2.18}$$

A similar process undertaken with respect to y yields a similar equation, less the surface shear and x component of gravity terms:

$$v = \frac{-1}{\mu}\left[(Nh - \sigma(\nabla^2 h))_y\right](\frac{1}{2}z^2 - hz) \tag{2.19}$$

In order to arrive at an equation describing only the height of the fluid, we apply conservation of mass to an element of the fluid, as shown below. As Δx and

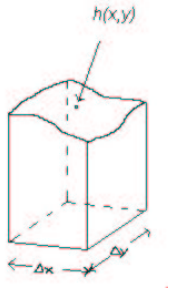

Figure 2.1: A volume element

Δy approach zero, the volume of the element can be approximated as $h(x,y)\Delta x\Delta y$. We now satisfy conservation of mass for an incompressible fluid (2.12), and write that the time rate of change of volume of the fluid element ($\frac{\partial V}{\partial t}$), is simply the net flux of the fluid crossing the faces of the element. Mathematically, this can be expressed as

$$\frac{\partial V}{\partial t} = \Delta y \int_0^{h(x-\frac{\Delta x}{2},y)} u\,dz - \Delta y \int_0^{h(x+\frac{\Delta x}{2},y)} u\,dz \tag{2.20}$$

$$+\Delta x \int_0^{h(x,y-\frac{\Delta y}{2})} v\,dz - \Delta x \int_0^{h(x,y+\frac{\Delta y}{2})} v\,dz \tag{2.21}$$

Dividing through by $\Delta x\Delta y$ and taking limits, we see that this is equivalent to

$$\frac{\partial h}{\partial t} = -\left(\int_0^h u\,dz\right)_x - \left(\int_0^h v\,dz\right)_y \tag{2.22}$$

Substituting in our previously derived expressions for u and v and evaluating the definite integral, we arrive at

$$h_t = \frac{-1}{\mu}\left[\left[\left[-\left(M + (-Nh + \sigma\nabla^2 h)_x\right)\right](-\frac{h^3}{3}) + \frac{C}{2}h^2\right]_x + \left[\left[(Nh - \sigma\nabla^2 h)_y\right](-\frac{h^3}{3})\right]_y\right] \tag{2.23}$$

which can be rearranged as

$$h_t = \frac{1}{\mu}\left[\nabla \cdot \left[\frac{h^3}{3}\nabla(Nh - \sigma\nabla^2 h)\right] + \left(\frac{Mh^3}{3} + \frac{Ch^2}{2}\right)_x\right]. \tag{2.24}$$

This PDE is our equation of interest which describes the height of the fluid as it evolves in time and space. Here we can see different forces accounted for in the different terms of the equation. The term containing N represents the vertical component of gravity, which is maximum when the the surface is flat, and zero when it is vertical. The term containing σ is the surface tension term, while the M term accounts for the horizontal component of gravity, and the C term accounts for surface shear. In the next section we aim to reduce the parameter dependence of the equation in order to analyze it more easily.

2.3 Nondimensionalization

We seek to facilitate the exploration of the droplet behavior by minimizing the number of dynamic variables involved, which we achieve through the process of nondimensionalization. Thus recognizing differing length scales for length in the x direction and for height in z, we nondimensionalize as follows:

$$h = H\tilde{h},\ l = L\tilde{l},\ t = T\tilde{t}, \tag{2.25}$$

where the capital letters are the dimension carrying terms. For notational convenience we drop the tilde, and remember that every variable below is now dimensionless.

$$h_t = \nabla \cdot \left[h^3\nabla\left(\frac{TNH^3}{3\mu L^2}h - \frac{T\sigma H^3}{3\mu L^4}\nabla^2 h\right)\right] + \left(\frac{TMH^2}{3\mu L}h^3 + \frac{TCH}{2\mu L}h^2\right)_x \tag{2.26}$$

If, in non-dimensionalizing, we choose to make the time scaling of equal order as the shear stress term (and thus scale all other terms with respect to that), we have $T \sim \frac{2\mu L}{CH}$, and

$$h_t = \nabla \cdot \left[h^3 \nabla \left(Gh - S\nabla^2 h\right)\right] + \left(\Gamma h^3 + h^2\right)_x \tag{2.27}$$

where G the term originates from the z component of gravity, the S term accounts for surface tension effects, the Γ term accounts for the x-component of gravity, and the unmodified term is the surface shear term, to which all other terms are normalized. The form of the remaining scaling terms is

$$G = \frac{2H^2N}{2LC} \tag{2.28}$$

$$S = \frac{2\sigma H^2}{3CL^3} \tag{2.29}$$

$$\Gamma = \frac{2MH}{3C} \tag{2.30}$$

To further nondimensionalize, we set $H = \sqrt{\frac{3LC}{2N}}$. This gives

$$G = 1 \tag{2.31}$$

$$S = \frac{\sigma}{L^2 N} \tag{2.32}$$

$$\Gamma = \sqrt{\frac{2LM^2}{3CN}} \tag{2.33}$$

Finally, setting $L = \sqrt{\frac{\sigma}{N}}$, we have

$$G = 1 \tag{2.34}$$

$$S = 1 \tag{2.35}$$

$$\Gamma = (\frac{2}{3C})^{\frac{1}{2}} \sigma^{\frac{1}{4}} N^{\frac{-3}{4}} M \tag{2.36}$$

Our final equation is then of the form

$$h_t = \nabla \cdot \left[h^3 \nabla \left(h - \nabla^2 h\right)\right] + \left(\Gamma h^3 + h^2\right)_x \tag{2.37}$$

We seek to examine the behavior of a droplet subject to this equation under varying size, shape, and values of Γ. In addition, we will consider the one-dimensional

form of the equation as well, and compare simulations from one and two dimensions. The one dimensional form is simply

$$h_t = \left[h^3(h - h_{xx})_x + \Gamma h^3 + h^2\right]_x \tag{2.38}$$

Neither of these equations are analytically tractable, and this requires that we use a numerical solver. We discuss ours in the next chapter.

Chapter 3

Numerical Methods

Both the one-dimensional and two-dimensional forms of the relevant thin film equation are clearly difficult to solve which requires numerical techniques. We discuss our methods below.

3.1 Discretization and iteration techniques

We discretize the 2-d equation using a centered finite difference scheme and a fully implicit time step. For convenience, we break it into a system of two equations, making the substitution $f = \nabla^2 h$. This gives us a system

$$H_{i,j} = \frac{h_{i,j} - h^n_{i,j}}{\Delta t} + G_{i,j} + S_{i,j} + \Gamma_{i,j} + C_{i,j} = 0 \tag{3.1}$$

$$\begin{aligned} F_{i,j} &= f_{i,j} - \frac{1}{(\Delta x)^2}\left(h_{i+1,j} - 2h_{i,j} + h_{i-1,j}\right) \\ &\quad - \frac{1}{(\Delta y)^2}\left(h_{i,j+1} - 2h_{i,j} + h_{i,j-1}\right) = 0, \end{aligned} \tag{3.2}$$

where

$$\begin{aligned} G_{i,j} &= \frac{G}{8(\Delta x)^2}\left[(h_{i+1,j} + h_{i,j})^3(h_{i+1,j} - h_{i,j}) - (h_{i,j} + h_{i-1,j})^3(h_{i,j} - h_{i-1,j})\right] \\ &\quad + \frac{G}{8(\Delta x)^2}\left[(h_{i,j+1} + h_{i,j})^3(h_{i,j+1} - h_{i,j}) - (h_{i,j} + h_{i,j-1})^3(h_{i,j} - h_{i,j-1})\right] \end{aligned} \tag{3.3}$$

$$\begin{aligned} S_{i,j} &= \frac{S}{8(\Delta x)^2}\left[(h_{i+1,j} + h_{i,j})^3(f_{i+1,j} - f_{i,j}) - (h_{i,j} + h_{i-1,j})^3(f_{i,j} - f_{i-1,j})\right] \\ &\quad + \frac{S}{8(\Delta x)^2}\left[(h_{i,j+1} + h_{i,j})^3(f_{i,j+1} - f_{i,j}) - (h_{i,j} + h_{i,j-1})^3(f_{i,j} - f_{i,j-1})\right] \end{aligned} \tag{3.4}$$

$$\Gamma_{i,j} = \frac{\Gamma}{8\Delta x}\left[(h_{i+1,j} + h_{i,j})^3 - (h_{i,j} + h_{i-1,j})^3\right] \tag{3.5}$$

$$C_{i,j} = \frac{1}{4\Delta x}\left[(h_{i+1,j} + h_{i,j})^2 - (h_{i,j} + h_{i-1,j})^2\right] \tag{3.6}$$

and subscript denotes the spatial gridpoint. Since this is a fully implicit scheme, all entries are taken to be at time $n+1$ unless explicitly noted in the superscript (as in $h_{i,j}^n$).

In a fully implicit discretization of a nonlinear system such as this, we guess at a solution and Newton iterate until we converge to a solution that satisfies the system of equations. In order to guarantee convergence (within an appropriate region), we construct the following linear system:

$$\begin{pmatrix} H_1 \\ F_1 \\ H_2 \\ F_2 \\ \vdots \\ H_N \\ F_N \end{pmatrix} + \begin{pmatrix} \frac{dH_1}{dh_1} & \frac{dH_1}{df_1} & \frac{dH_1}{dh_2} & \frac{DH_1}{df_2} & \dots & \dots & \dots \\ \frac{dF_1}{dh_1} & \frac{dF_1}{df_1} & \frac{dF_1}{dh_2} & \frac{DF_1}{df_2} & \dots & \dots & \dots \\ \frac{dH_2}{dh_1} & \frac{dH_2}{df_1} & \frac{dH_2}{dh_2} & \frac{DH_2}{df_2} & \dots & \dots & \dots \\ \frac{dF_2}{dh_1} & \frac{dF_2}{df_1} & \frac{dF_2}{dh_2} & \frac{DF_2}{df_2} & \dots & \dots & \dots \\ \dots & \dots & \dots & \dots & \ddots & \dots & \dots \\ \dots & \dots & \dots & \dots & \dots & \frac{dH_N}{dh_N} & \frac{dH_N}{df_N} \\ \dots & \dots & \dots & \dots & \dots & \frac{dF_N}{dh_N} & \frac{dF_N}{df_N} \end{pmatrix} \begin{pmatrix} \Delta h_1 \\ \Delta f_1 \\ \Delta h_2 \\ \Delta f_2 \\ \vdots \\ \Delta h_N \\ \Delta f_N \end{pmatrix} = \mathbf{0}$$

where $N = mn$ is the number of gridpoints (assuming n rows and m columns), and each gridpoint is assigned the number $jn + i$. Solving this system gives us a vector containing approximate corrections Δh_i and Δf_i which we add to each h_i and f_i, and use the result as our guess for the next time step. We then reconstruct the system and solve it again. We continue to modify the h and f vectors in this fashion until the norm of the correction vector is below some tolerance. Satisfaction of this tolerance signifies that h and f are no longer changing significantly, so the current values are then accepted as one time step, and the process is repeated with the new solution becoming the guess for the next time step. For further information on finite difference methods and Newton iteration, see Burden and Faires [1].

Numerically, we take advantage of the fact the Jacobian matrix above is banded, with half-bandwidth $= 2n + 1$. Thus, for a 100 by 100 grid, we would have 10000 gridpoints with a Jacobian of 400 million points, of which 8060000 are stored. It

should be noted that even in this banded form, the majority of entries are zeros because there is a solid diagonal of half-bandwidth 3 down the center, and then one superdiagonal and one subdiagonal each $2n$ away (these result from the mixed derivative). In between these diagonals are only zeros. If the terms involving the outer diagonals could be approximated in some manner, it is possible significant improvement in speed could be had, assuming that the reduced rate of convergence was offset by the increased speed in solving the matrix system.

The code for solving the one-dimensional version of the equation (actually written first) works by the same method, with only the discretization being different: Any term that involves derivatives in the y direction simply becomes zero. Since there is only one 'row,' points are labeled straightforwardly and N just equals n. This program runs much much faster, since the system being solved is of size $2n$ with half-bandwidth of just 3. For more discussion of the code, see the appendix.

3.2 Precursor film

It should be mentioned that when numerically modeling a free surface of a fluid contacting a solid surface (as is the case with a droplet or the front of a thin film), the typical no-slip condition on which the equations were derived would not allow the contact line to advance. This is because all terms in the PDE are a function of height, and when this is zero, h_t is always zero.

There exist two standard methods of circumventing this issue. One is a Navier-slip method which relaxes the no-slip condition very near the contact line, advancing it based on the behavior of the rest of the free surface. The other method (which we adopt) is to use what is called a precursor film. Numerically, this exists as a flat sheet of fluid with height at least an order of magnitude less than the height of the drop. The relatively small height prevents excessive diffusion of the drop or film, yet allows the object of interest to change it's boundaries. A precursor film

cannot give a completely accurate representation of the drop since diffusion will always be playing a role at the boundaries even when it should not be, however it is computationally much simpler and faster, and in many cases gives (for thin films at least) approximately the same results [3].

3.3 Numerical verification

Tests were run to confirm that the code preserved volume, that the dynamic time step did not yield significantly different results than the fixed time step, and that varying grid density did not have significant effects. It was found that volume was preserved within 10^{-6} of the original volume, that for the 1-d code the dynamic time-step advanced 3 gridpoints (out of 500) farther of a long-time run, and that when shifted to account for that movement, differences in height at gridpoints were on the order of 10^{-3}. None of these indicate a need for concern with the numerical functioning of the system.

Chapter 4

Results

In an effort to examine what governs the behavior of moving droplets, we implemented the numerical solvers to solve the one dimensional form,

$$h_t = \left[h^3(h - h_{xx})_x + \Gamma h^3 + h^2\right]_x, \tag{4.1}$$

and the two-dimensional form,

$$h_t = \nabla \cdot \left[h^3 \nabla \left(h - \nabla^2 h\right)\right] + \left(\Gamma h^3 + h^2\right)_x, \tag{4.2}$$

of our equation which describes droplet height as a function of time and space. Specifically, we looked at what droplet shapes evolve, and how they differ as a function of drop size, shape, and variations in the parameter Γ. We also ran various checks to test the validity and applicability of our model to our long-term goal of modeling coalescing droplets on the surface of a wing.

4.1 Droplet phases

We begin our discussion of simulation results with a description of the qualitative phases through which a shearing drop progresses. Our simulations all began with a Gaussian-like initial condition, the general form of which is shown in figure 4.1. This was generated by allowing a spherical cap to diffuse free of shearing forces until the radial velocity of the edge of the drop had fallen off considerably (since the drop is on a precursor film it will never completely cease spreading and some cutoff must be subjectively decided upon).

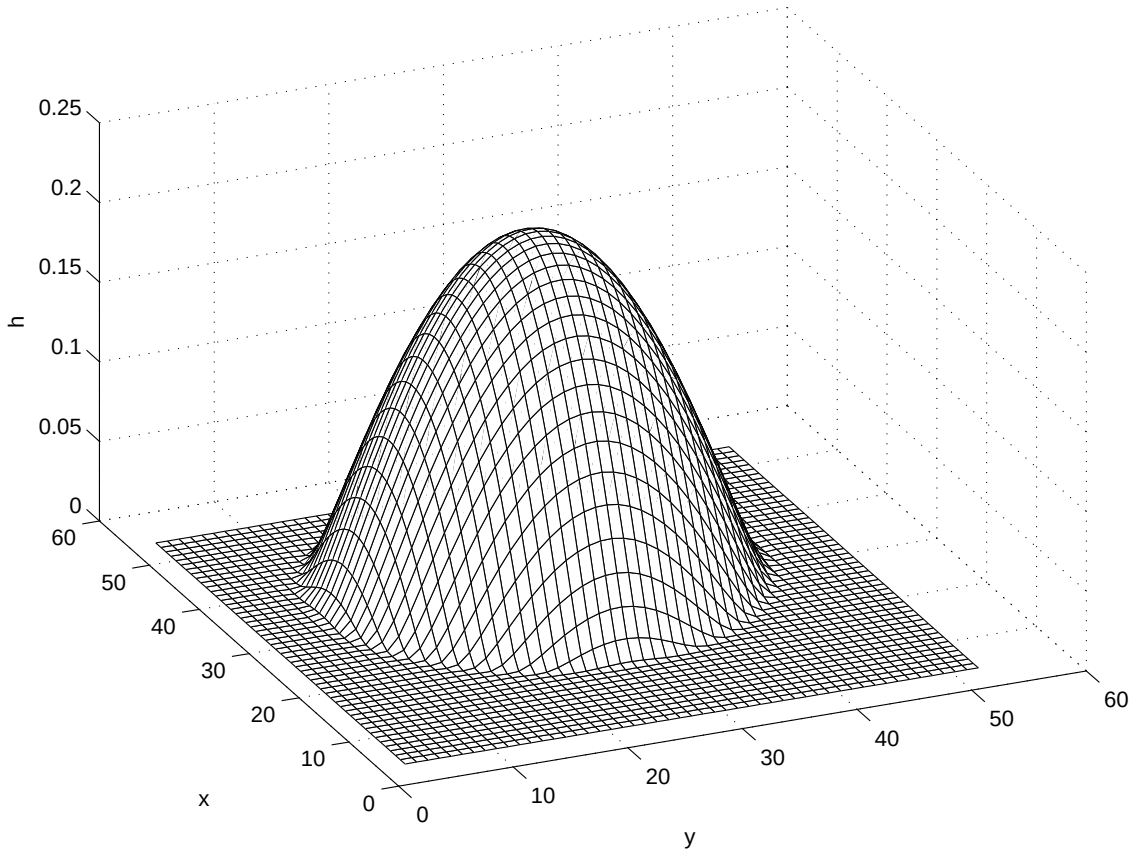

Figure 4.1: The form of a typical initial condition drop.

The first qualitative stage the droplet goes through is simply a generally shifting of this initial condition. With the exception of where it meets the precursor film, the surface remains everywhere convex, with the downwind side just steepened and the center of mass shifted in the direction of positive x as can be seen in figure 4.2.

After this, the drop develops somewhat of a flattened back and takes on what might be called a rounded tetrahedron shape, where the edges are composed of the contact lines, and those bounding the 'back face' of the drop, shown in figure 4.3.

We saw in the tetrahedron figure a tip developing at the front of the drop. As we progress in time, the tip becomes more and more pronounced. Here, in 4.4 we see this pronounced tip, as well as a dimple beginning to form behind it.

This dimple is the beginning of what can be labeled a crescent-shaped phase of the droplet, where the curved front of the drop rises above the inner portions, creating a crescent-shaped concavity in the back of the drop. This general phenomenon can be observed when blowing water droplets along glass surfaces. Figure 4.5 displays a more fully developed crescent shape.

Also in this figure, the tip can be seen to extend beyond the front of the drop, forming a longitudinal ridge as well. What occurs beyond this point is unclear, as more runs need to be performed out in this phase of the droplet behavior. What has happened in a few cases is that the tip continues thinning longitudinally, to the point that in the x-direction it is described by only a few gridpoints, as shown in figure 4.6. This may be a numerical artifact which would disappear with finer grid resolution, or may be the numerical manifestation of some other phenomenon such as droplet overturning.

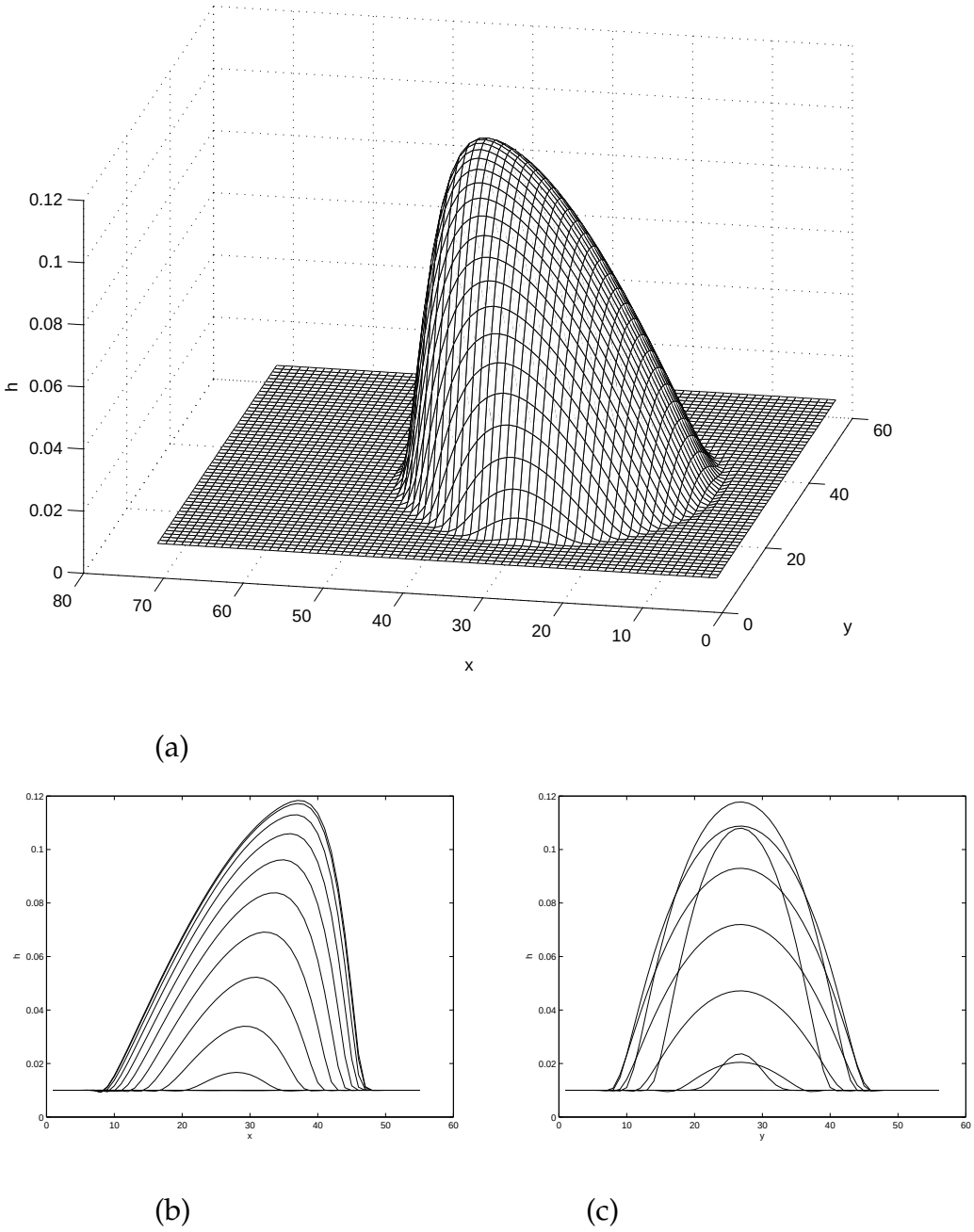

Figure 4.2: a) shows a 2-d view of the deformed drop after time $t = 3.7$. b) and c) show cross-sections in x and y.

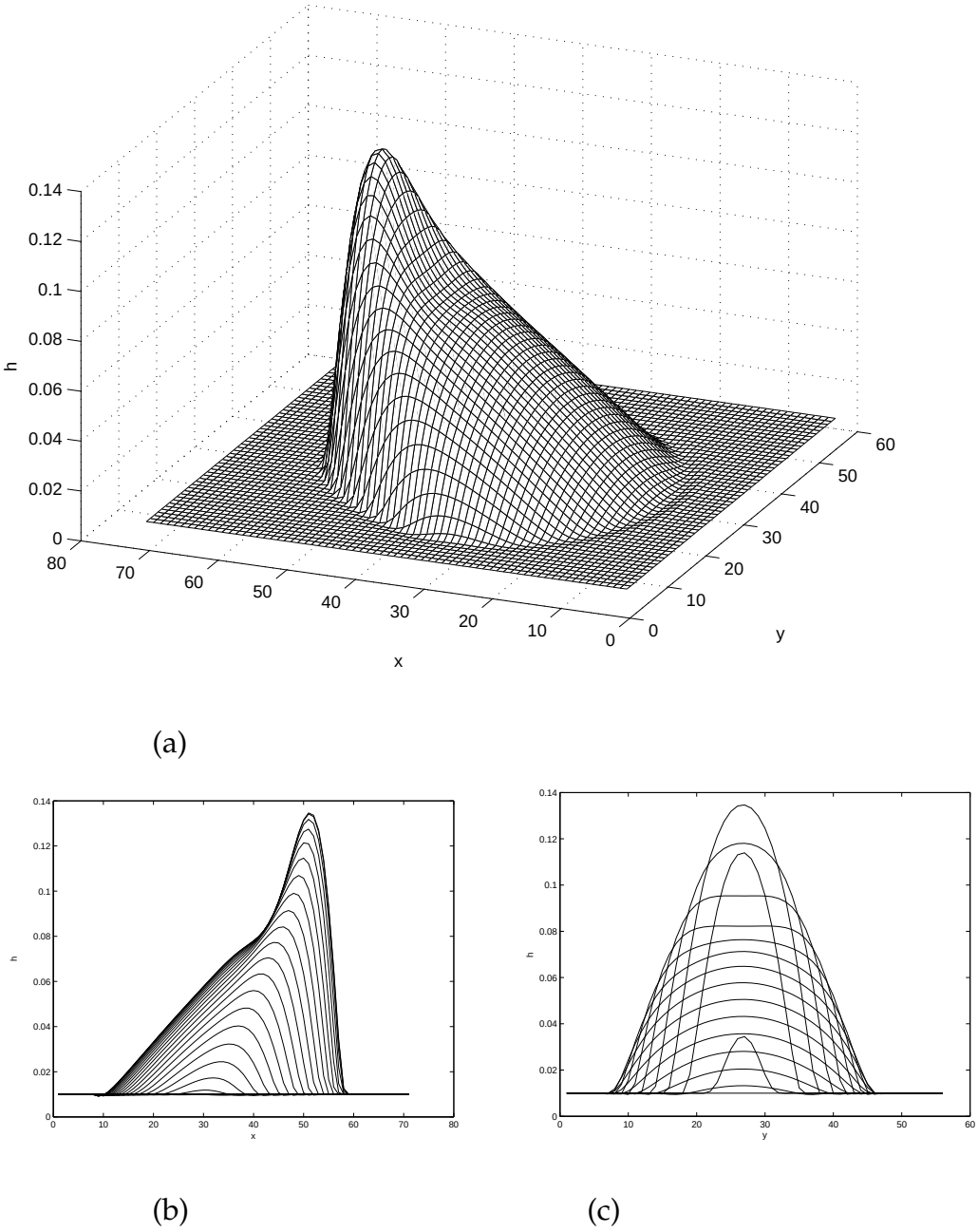

Figure 4.3: a) three dimensional representation at time $t = 13.5$. b) and c) show cross section in x and y.

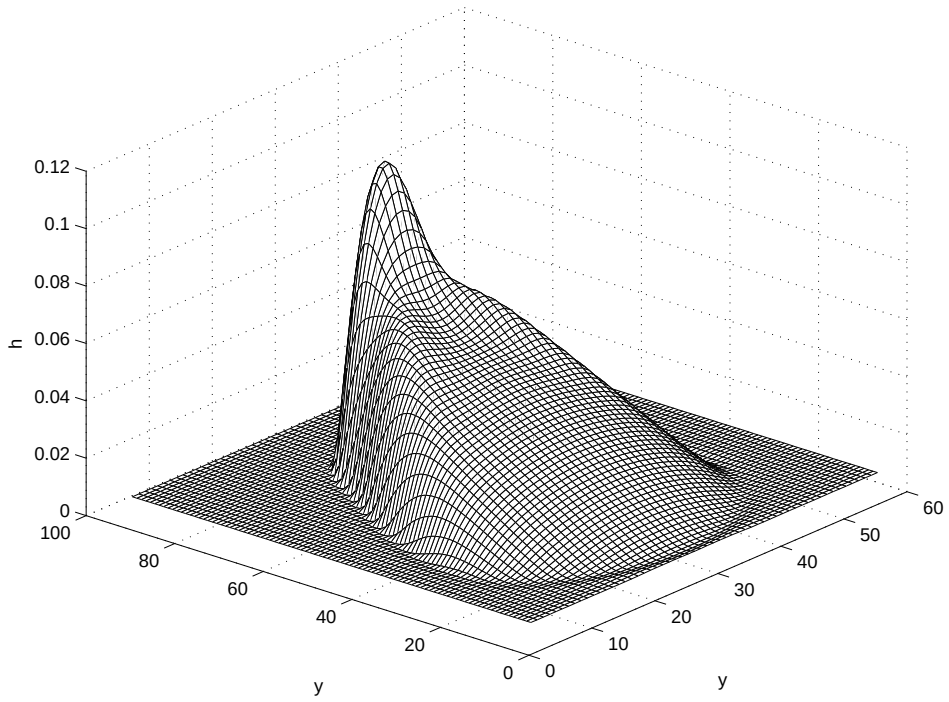

(a)

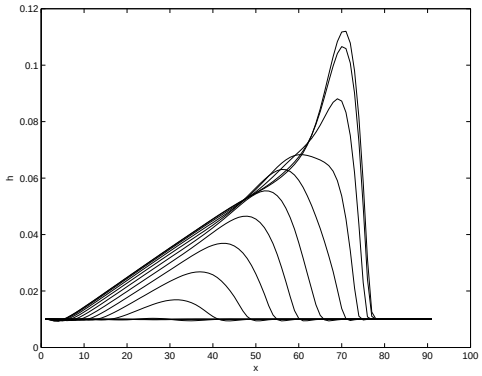

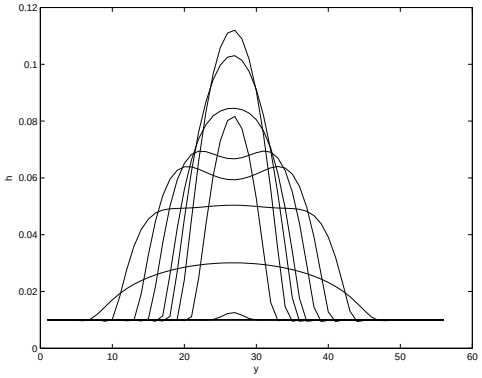

(b) (c)

Figure 4.4: a) 3-d representation at time $t = 39.5$. b) and c) are cross-sections in x and y. Note concavity in y cross-section.

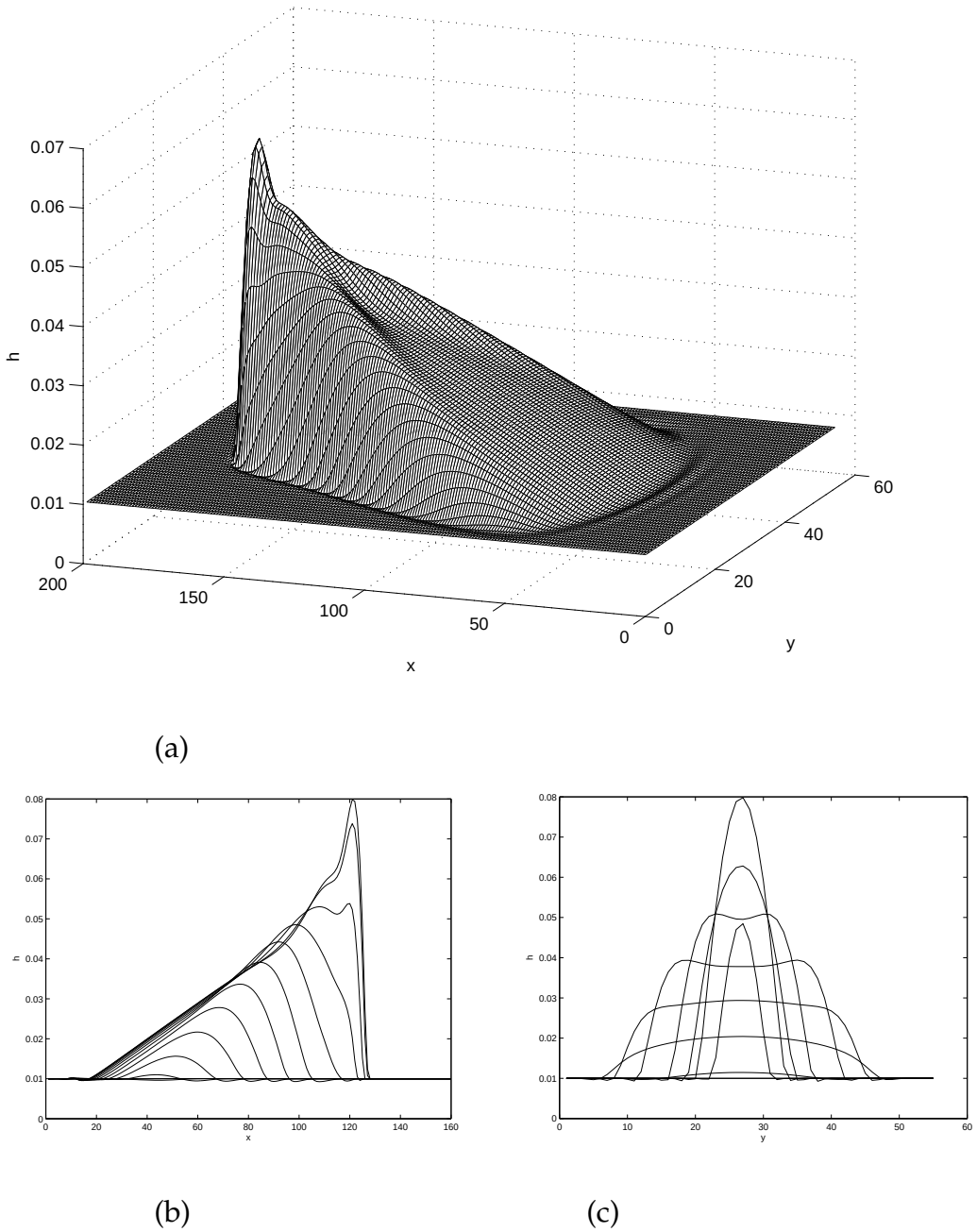

Figure 4.5: a) three dimensional representation of drop at time $t = 179$. Note longitudinal ridge behind tip. b) and c) are cross section in x and y.

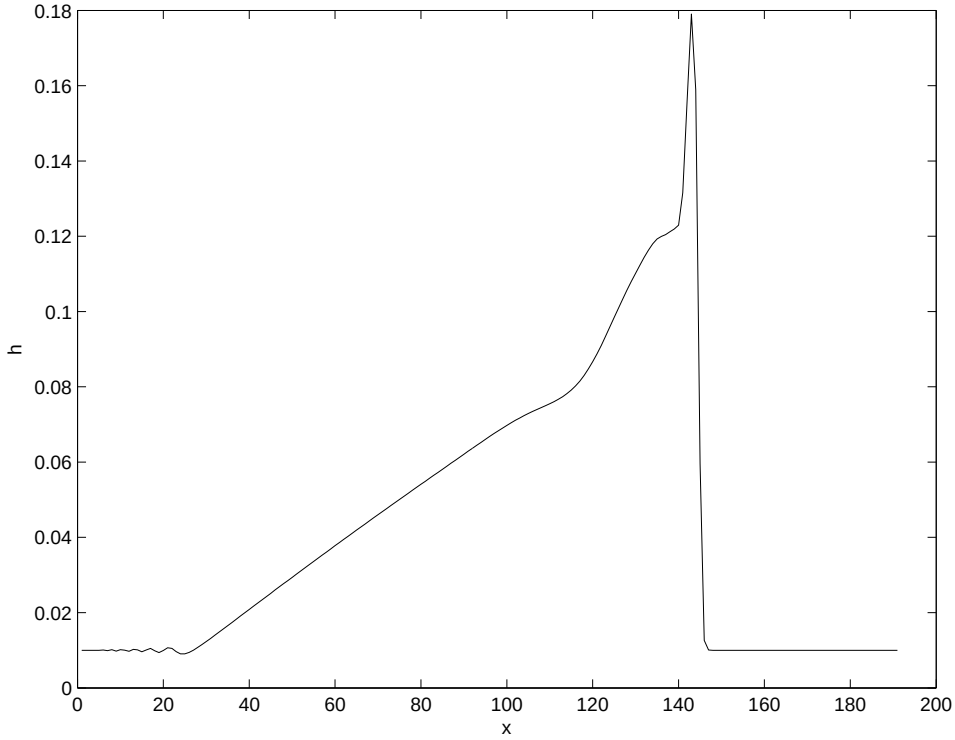

Figure 4.6: Note the extremely narrow width of the tip. Shortly after this time, the simulation ceases to function properly.

4.2 Parameter studies

Parameter studies were done, varying Γ, dx, and initial height, all independently, and also varying height and dx simulataneously by the same factor. Aside from a qualitative examination of the results, we measured the time it took to form a depression in the back of the drop, which was taken as a measure of how susceptible the drop is to shear-induced deformation. The standard run to which comparisons were made had a dx of $.1$, and an initial height of $.23$. Our results are summarized in the chart below. Each pair of columns gives the time to depression formation for the given paramater value, or in the case of h_0 and size variation, the scaling of the reference initial condition.

Γ	t		dx	t		h_0	t		size	t
1	9.6		.05	42.3		.5	12.2		.5	31.7
2	6.7		.1	9.6		1	9.6		1	9.6
4	3.9		.4	7.8		2	8.69			

Runs were performed on a wider range of parameters, however due to various numerical issues not all of them gave useful data. We can at least reach tentative conclusions from the data we do have. We find that, not surprisingly, a stronger driving force decreases the time to becoming crescent shaped, and that widening the drop does the same. When changing both the height alone as well as the size of the drop however, we find that the smaller the drop, the more stable it is - that is, the longer it takes for a depression to form. This probably is a result of surface tension being able to keep the surface more uniform as its relative contribution increases the smaller the drop becomes, since curvature necessarily becomes greater.

4.3 Two drop coalescence

Since the motivation behind the project involves modeling the behavior of shearing droplets which coalesce, a check was made to ensure the droplet coalescence does not present any special simulation problem. We placed two droplets within close proximity, so that after a small amount of time they would diffuse into each other, at which point we would expect surface tension effects to more quickly bring the drops together. This is indeed what occurred, as can be seen in figure 4.7. However, it is not visually obvious from these results that surface tension is in fact bringing the drops together more quickly than would occur were the drops just diffusing without interaction. Thus we ran a single drop diffusion to an equal time and superimposed the resulting profiles. This clearly shows the interface height is being raised much more quickly when the drops are interacting. This, combined with the fact that a precursor film eliminates a need to track the qualitative difference of whether two drops have touched, indicates that our model is both a convenient and capable means for simulating droplet coalescence on a larger scale.

4.4 Inevitable shear dominance

Examining the governing equation of our system, one can see that since the shear and x-gravity terms are $(h^2)_x$ and and $(h^3)_x$ respectively, the shear term will dominate for heights significantly less than one. While this does model a physical reality, when it is combined with a precursor film model in which droplets leave tails and continually expand outwards, it implies that there will be inevitable shear dominance of the drop. This is because all drops will spread out and subsequently (by conservation of mass) decrease in height, and at some point the drop will move in the direction of shear, regardless of which direction gravity is driving it. Indeed, we see this phenomenon in figure 4.8. This is a one-dimensional run, where the profile is displayed changing through time. Gravity is set working to the right,

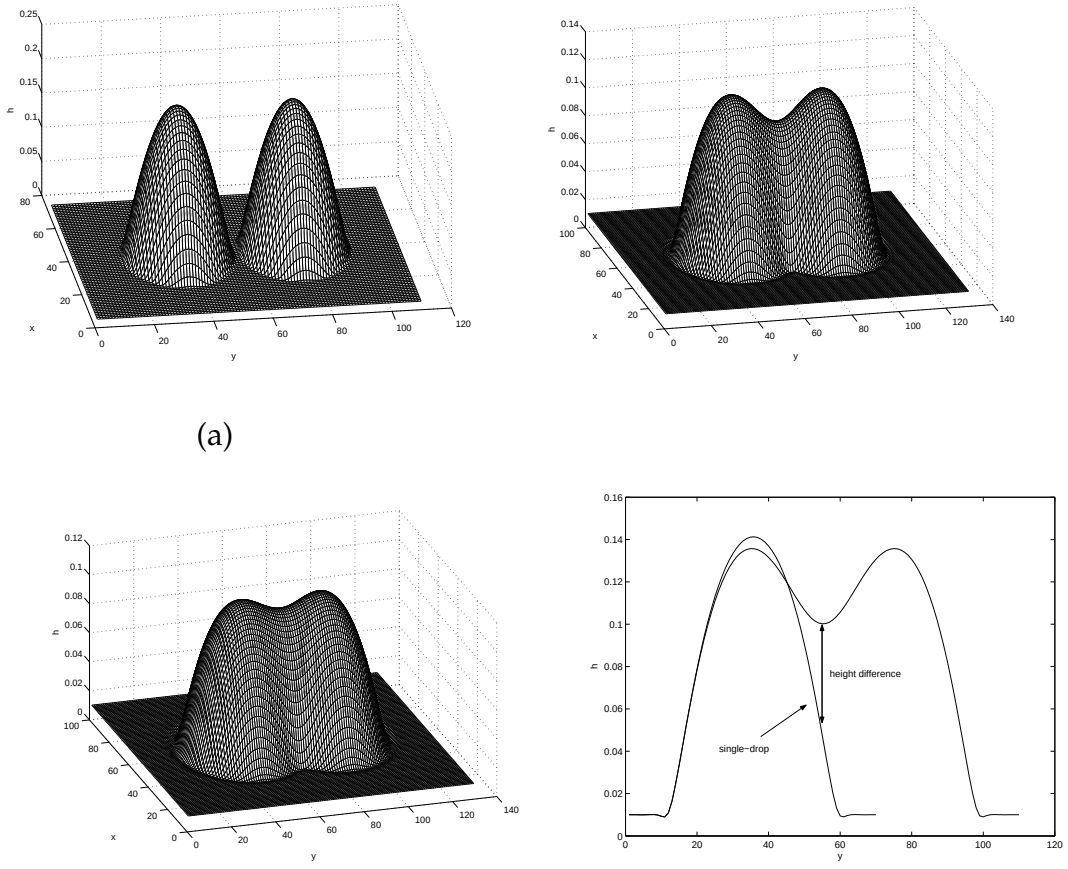

(a)

(b)

(c)

Figure 4.7: a) double drop initial condition. b) partial merger. c) more complete merger. d) distinguishing merger surface tension effects.

while shear is directing the drop to the left. We see that while the drop is tall, the peak moves toward the right, but eventually the entire drop is driven in the opposite direction. It should be noted that this is a limitation in applicability of the model, rather than an inherent flaw, as the phenomenon of flow reversal can be seen when a large drop of fluid flows down a windshield, spreading into a rivulet which undergoes flow reversal once sufficiently drawn out. To properly apply our model, one must either be modeling a drop which does in fact leave a trail, or only consider results obtained before the drop has spread significantly.

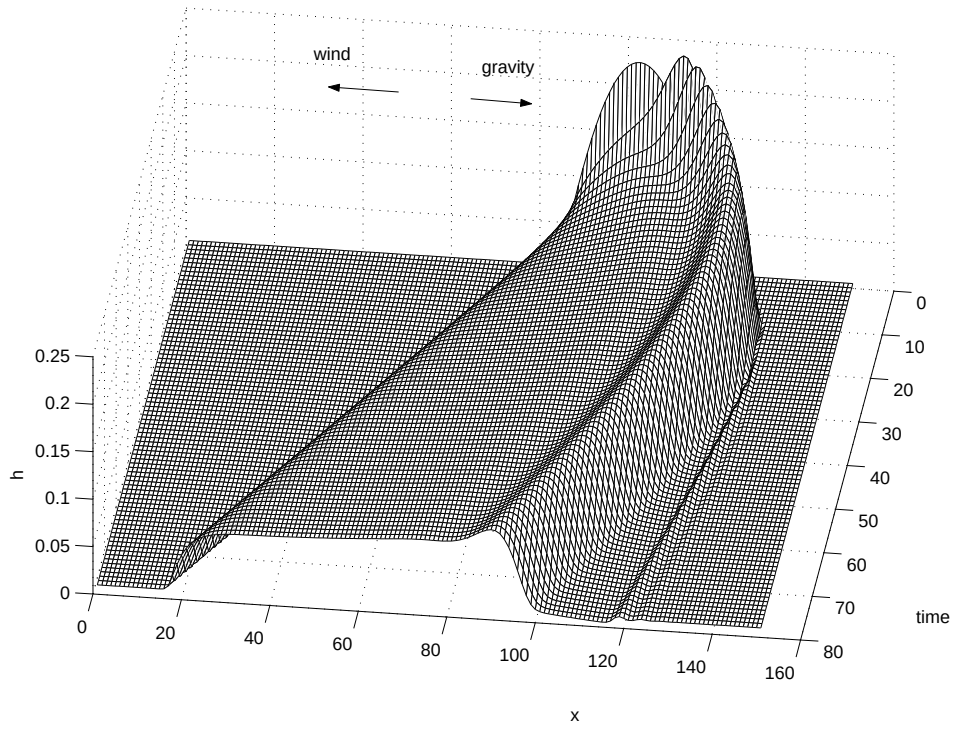

Figure 4.8: This plot shows a one-dimensional droplet evolving over time. It initially moves to the right, but as it spreads out shear dominates and it gets sent in the opposite direction.

4.5 Comparison of 1-d and 2-d simulations

As mentioned in the introduction, work has previously been done by sauthors modeling droplets height as a function of a single spatial dimension only. Another aim of our project was to compare the results of simulation in one and two spatial dimensions to see whether one-dimensional modeling (which is computationally much simpler) can give useful insight into real droplet behavior, whether there are qualitative features it cannot capture, and what factors need to be borne in mind when doing 1-d droplet modeling.

To compare results, we set the center longitudinal profile of the 2-d initial condition as the initial condition for the 1-d simulation, and set both Γ and dx to the same values for the one and two dimensional simulation. Each droplet was then run to various fixed times and the resulting profiles compared.

Examining figure 4.9, we can see that the droplet profile remains roughly the same, and moves at very nearly the same velocity. While in the first plot the 2-d drop profile has lost a slight amount of cross-sectional area due to outward diffusion in the y-direction, at a later time it appears to have gained in mass (indeed, integration over the vector determines that it has). The 1-d droplet meanwhile, conserves mass in both cases.

While differences in the center profile of the drop may not be significant, there is another issue to be examined. If we take longitudinal cross-sections of a 2-d drop we find profiles that would be very unlikely (if not impossible) to develop in a simple 1-dimensional simulation. As shown in figure 4.10, we find odd profiles with unusual concavities that mostly likely can only originate from the combined effects of forces in the x and y directions. This implies that it is not feasible to capture all the relevant features of droplet behavior simply using a one-dimensional model. It appears however, that 1-d modeling will give a surprisingly accurate estimate of the bounds for the center profile of a corresponding two dimensional drop.

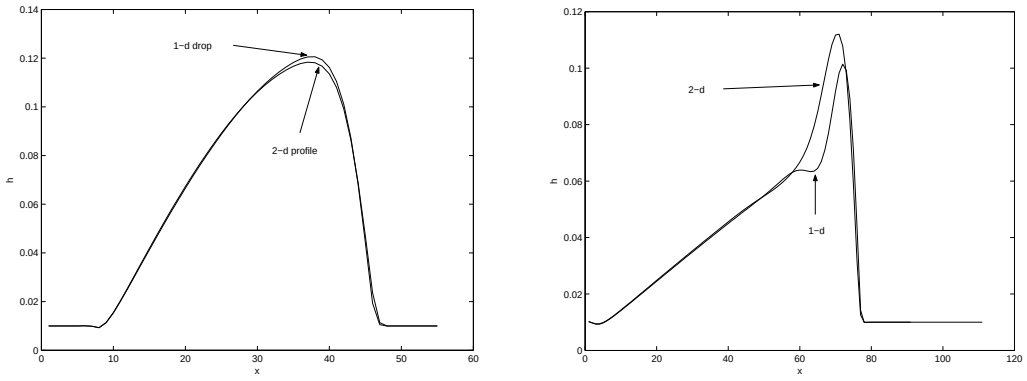

(a) (b)

Figure 4.9: Here we compare the central profile of a 2-dimensional drop with a simple 1-d run at two fixed times (a) = 3.7 and b) = 39.6).

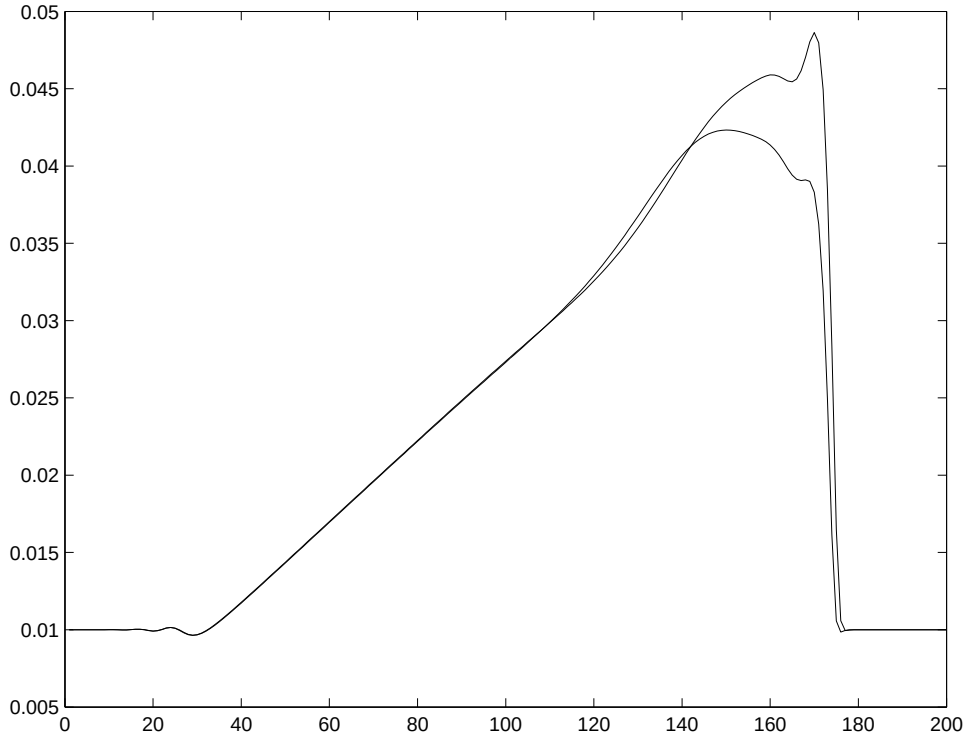

Figure 4.10: These plots are longitudinal cross-sections of a 2-d drop taken off the centerline. They show profiles which are likely impossible to get using the 1-d model.

4.6 Potential surface roughness modeling

In a thin film application, Kondic and Diez [7] modeled patterned surface roughness by patterned variations in precursor film height. Such variations in roughness can have the effect of altering contact angle, and if a drop lies across a boundary where one side has a lower contact angle, the drop will tend to move toward that side. This is a potential method for controlling droplet behavior on the surface of a wing. If our model is to be used to investigate the possibility of controlling droplet trajectories by altering surface roughness, we need to confirm that changes in the height of the precursor film do in fact result in altered drop trajectories. To check whether this was plausible, we ran a zero shear 1-d simulation on a symmetric drop, where the precursor film was of height $.01$ to the right of the drop, and $.02$ to the left of the drop. The results can be seen in figure 4.11. A mild skew to the left can be seen as compared with the initial condition, though it is very slight compared to the diffusion in both directions. We can however, check that the location of maximum height did in fact shift to the left by two gridpoints. The effect then, is real, though a systematic study characterizing the relations between precursor film height, droplet steepness and velocity of diffusion would need to be performed to determine whether changes in surface roughness (or numerically, precursor film height) could be used to effectively guide drops.

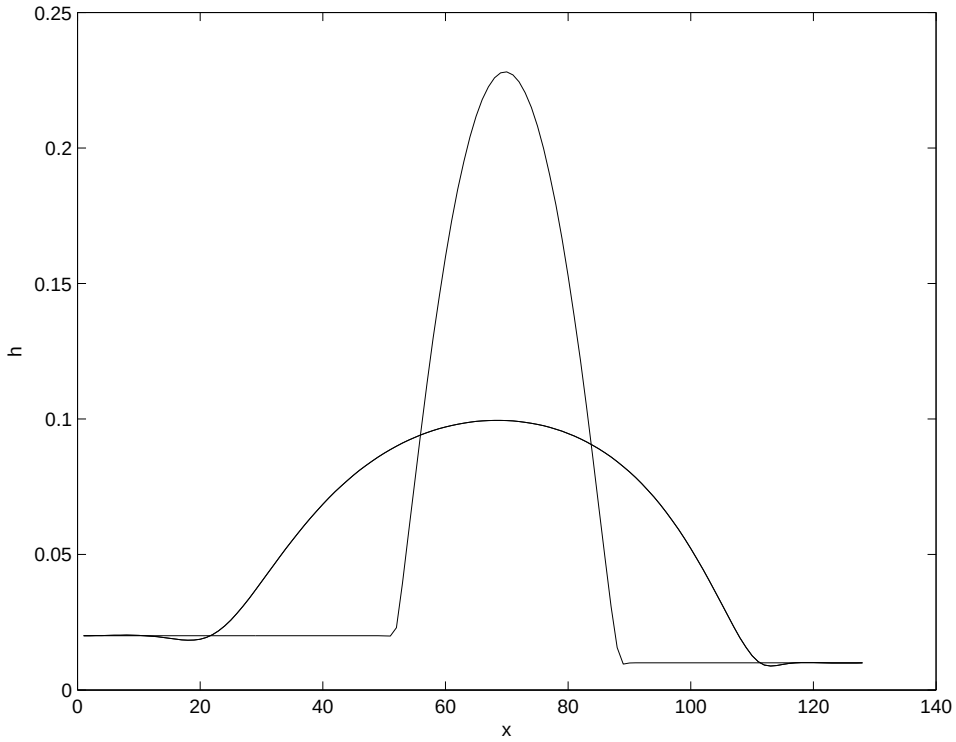

Figure 4.11: This plot illustrates the (slight) effect differing precursor film heights can have on an otherwise symmetric drop. The drop has spread out and moved slightly to left, in the direction of the higher precursor film.

Chapter 5

Conclusions and Future Work

We successfully simulated droplet deformation as a result of gravity and surface shear, in both one and two dimensions. We were able to characterize general droplet behavior, as well as describe the effect of changing the driving force and size and shape of the droplet. We were able to investigate the applicability and limitations of our precursor film model, and found that while the inherent diffusion involved places limits on the applicability of certain results, our model should be suited to further modeling of more complex droplet interactions, such as may be found on the surface of a wing in rain. We also successfully compared runs of one and two-dimensional drops and found that while the 1-d model matches quite closely the front and back edges of a two-dimensional drop, there are certain qualitative features which 1-dimensional modeling cannot capture.

If the project were to be continued, it is recommended that the 2-dimensional code be converted to use an Alternating Direction Implicit method (ADI), which, as described in Witelski and Bowen [16], greatly decreases computational time, by changing the problem to one which involves solving many much smaller matrix equations as opposed to one large one. Once this is done, more systematic study of both large scale coalescence as well as the ability to control droplet trajectory through variations in precursor film height could be undertaken. It might also be wise to investigate methods for realistically handling the inevitable diffusion caused by the use of a precursor film.

Lastly, a lofty goal to be kept in mind in is that of simulation of the film formation and break up process. Ideally by starting with a randomized array of droplets

we could observe mass coalescence into a film, followed by film breakup and rivulet formation due to instability. Combined with explorations into changing droplet trajectory, such a model could give both theoretically interesting insights, as well as information useful from an engineering standpoint.

Appendix A

Appendix

A.1 Discussion of Code

Code for solving the one dimensional version of our equation was written in Matlab in the summer of 2002. In the fall, it was deemed necessary to convert the code to C both because it would drastically improve the speed of 1-d simulation, and also because it would be necessary to make 2-d simulation practical at all. The plan for some time was to use an ADI method for the 2-d code, however timeline issues and the intricacies involved led to the development of a clumsier but more easily implementable 2-d code which operates on the same principles as the 1-d code. As discussed in chapter 3, it involves a banded matrix who's half bandwidth is twice the number of gridpoints in the x-direction, and who's length is two times the total number of gridpoints. The matrix solving is by far the limiting step in the speed of our program, and scales strongly with halfbandwidth, and thus with the number of gridpoints in the x-direction. Currently, the step takes on the order of 1 to 20 seconds, depending upon both the gridsize as well as the smoothness of the surface being modeled. The 1-d C code can run though tens of time steps per second. Thus switching to ADI would very likely decrease the computational time.

Since they use similar methods, the 1-d code and the 2-d code each have a similar structure with similar supporting files. Both use a vector class, a matrix class and an 'smatrix' class (the two are equivalent in the 1-d code), all of which were written specifically for the program. The vector class performs useful functions

such as finding the norm of the vector as well as reading in and printing out vectors from ascii files. The standard matrix class provides a way of conviently referencing a gridpoints in the 2-d simulation, and can store matrices in both banded and full forms. The smatrix class is very similar to the matrix class, except it automatically produces an array whose entries are taylored so that it can be passed to the dgbsv Fortran banded matrix solver (documentation can be found by going to any search engine and typing dgbsv).

The main files for each are big2.c and big2d.c - these are written in a rather ugly script-like fashion, and the b vector, jacobian, solving, updating, time stepping and outputting all occur here. Each also has a file benparam.h, which contains constant information about the initial timestep, gridspacing, gridsize, and other parameter values.

When performing runs in either program, the following items must be noted: The initial condition vector to be read in is named near the top of big2.c and big2d.c. The name of the output vectors are changed at the bottom of those two files. The 2-d simulation outputs a vector of all the gridpoints, as well as a vector of the time and time step at each output. Attention must also be paid to adjusting the boundary conditions, both in constructing b (of $Ax + b = 0$) and in constructing the Jacobian.

Both codes have similar files plotfixer.m and antiplotfixer.m, designed for relating the output and input to matlab. In each case, plotfixer takes in the name of a run (which is output as a giant vector) as well as the gridsize (and in the case of 2-d, the time step to be visualized), and outputs a matrix. For the 1-d code, the rows are entries at given time, and time progresses through the columns. For 2-d code, it is at a specific time, and a mesh of the matrix will show the shape of the 2-d droplet.

Antiplotfixer.m takes a matrix and creates a vector with the columns appended in an appropriate fasion so that it can be read as an initial condition.

Lastly, ccavechecker.m takes a 2-d run and it's associated time vector and determines at what time concavity first appeared in the back of the drop. It does this by taking cross-sections in the y direction and seeing at what time the maximum is no longer in the middle of the profile.

In general, when viewed by a CS major, the code will likely appear ghastly and inelegant, and a knowledgeable person could likely make many improvements to increase it's ease of use. It does however, function.

Bibliography

[1] R.L. Burden and J.D. Faires. *Numerical Analysis*. PWS-Kent Pub. Co., 1993.

[2] B.A. Campbell and M. Bezos. Steady-state and transitional aerodynamic characteristics of a wing in simulated heavy rain. *NASA*, TP-2932, 1989. Describes the results of wind-tunnel experiments and the effect rain has on the aerofoil properties.

[3] J.A. Diez, L. Kondic, and A. Bertozzi. Global models for moving contact lines. *Phys. Rev. E*, 63, 2000. A paper justifying the use of precursor film models. It analyzes both slip models and precursor models, determining that for wetting films, precursor models perform just as adequately as slip models, and that precursor film models are computationally much more efficient.

[4] P. Dimitrakopoulos and J.J.L. Higdon. Displacement of fluid droplets from solid surfaces in low-reynolds-number shear flows. *J. Fluid Mech*, 336:351–376, 1997. 2-dimensional study drop displacement in Stokes flow. Claims to find that the usefulness of lubrication models is limited, and therefore will be useful to check with once our simulation is running.

[5] P.A. Durbin. On the wind force needed to dislodge a drop adhered to a surface. *J. Fluid Mech.*, 196:205–222, 1988. Solves for the shape of a droplet just before it is dislodged by the force of wind. Interesting, but not terribly useful.

[6] L. Kondic. Instabilities in gravity driven flow of thin fluid films. *SIAM Review*, 45(1):95–115, 2003.

[7] L. Kondic and J. Diez. Flow of thin films on patterned surfaces: Controlling the instability. *Physical Review E*, 65, 2002. This paper describes their technique of varying the precursor film height to simulate changes in surface topology, thereby controlling the wavelength of the thin film breakup. Will most likely use this method when controlling droplet behavior.

[8] X. Li and C. Pozrikidis. Shear flow over a liquid drop adhering to a solid surface. *J. Fluid Mech*, 1996.

[9] J.A. Moriarty and L.W. Schwartz. Unsteady spreading of thin liquid films with small surface tension. *Phys. Fluids A*, 3(5):733–742, May 1991. Uses an asymptotic matching method to model droplet flow down a wall or sheared by wind. Except the equations are the thin film equations for 1-d flow.

[10] T.G. Myers. Thin films with high surface tension. *Siam Rev.*, 40(3):441–462, September 1998.

[11] A.D. Schliezer and R.T. Bonnecaze. Displacement of a two-dimensional immiscible droplet adhering to a wall in shear and pressure-driven flows. *J. Fluid Mech*, 383:29–54, 1999. Studies the flow of a 2-d droplet between two plates in pressure driven or shear flow for adhered and slipping droplets.

[12] B.E. Thompson and J. Jang. Aerodynamic efficiency of wings in rain. *J. Aircraft*, 33(6):1047–1053, 1996. Describes experiments performed to determine the effects that altering wettability has on the aerodynamic performance of the wing.

[13] B.E. Thompson, J. Jang, and J.L. Dion. Wing performance in moderate rain. *J. Aircraft*, 32(5):1034–1039, 1995. This article documents other experiments

investigating the behaviro of wings in rain, including the effects of boundary layer tripping.

[14] B.E. Thompson and M.R. Marrochello. Rivulet formation in surface-water flow on an airfoil in rain. *AIAA Journal*, 37(1):45–49, 1999. Attempts to describe and predict the onset of rivulet formation in the convecting film on a wing by modeling it as occuring when the free-surface shear stress equals the stress at the liquid solid interface. Does not actually model fluid flow, though gives suprising agreement with experiment regarding the location of rivulet formation.

[15] S.K. Wilson, B.R. Duffy, and R. Hunt. A slender rivulet of a power-law fluid driven by either gravity or a constant shear stress at the free surface. *Q. Jl Mech. Appl. Math.*, 55(3):385–408, 2002. Introduction provides good background on the state of droplet modeling. Actual model is not 3-d, and mainly deals with profiles at different times.

[16] T.P. Witelski and M. Bowen. Adi schemes for higher-order nonlinear diffusion equations. *Pre-print*, June 2002. Describes the numerical method we plan to implement, and also gives examples of how to taylor it to specific equations.